STAR Note 187

December 31, 1994

REALISTIC ANALYTICAL MODEL OF XTPC PERFORMANCE; RECONSTRUCTION; SECONDARY REJECTION

James Draper, Lynn Wood, Juan Romero, Daniel Cebra, Paul Brady
Physics Department, University of California, Davis, California 95616

ABSTRACT

Analytical geometric solutions to the properties of the tracks in the STAR External TPC are derived and analyzed. A thin disk of radially increasing radial magnetic field following a cylinder of uniform axial magnetic field represents the field of the STAR solenoid. When the nonlinearity of the radial magnetic field is included, this model gives twist, radius and tracklength that match quite well, qualitatively and quantitatively, those we obtained using STAR GEANT. The model provides a quantitative understanding of the reason why the XTPC must be located as close as possible to the central TPC's magnet pole piece. The model is used to produce and analyze a quick, highly accurate method to reconstruct the pseudorapidity and momentum of each primary track over a wide range of momenta, <~0.2 to >~10 GeV/c. The model is also used to obtain a quick, highly selective method to eliminate the tracks of almost all secondary particles from the analysis. The analysis is made without multiple scattering. Tests with GEANT, including multiple scattering, are in progress.

The purpose of this investigation is to develop a model of the system of the central TPC of STAR at RHIC plus its external TPC (denoted XTPC) that is realistic, but also provides a framework in which to understand the properties of the real system, by virtue of analytic solutions of the model.

The trajectories of particles in the XTPC must ultimately be calculated by the program, GEANT, and we have done this in selected cases. However, GEANT is a complex program which sometimes gives results with significant uncertainty. For example, for the recommended mode of running, AUTO=1, results like the ones discussed below have substantial artificial scatter because of numerical problems in GEANT. This scatter is greatly reduced by running with AUTO=0 without inputing parameters to control the step length, but this increases the running time by almost an order of magnitude. One can make smaller programs, by truncating GEANT, but these still have problems of limited accuracy due to finite step length on the one hand, or roundoff errors when the step length is made too short. The present model is geometric and can quickly be calculated with accuracy $\sim 10^{-9}$.

Above is one reason for wanting a simple model of the system. A more important reason is that the model helps to develop understanding of the effects involved, and the means to handle them. For example, a detailed method is described here for reconstruction of each track to obtain the momentum and pseudorapidity as accurately as possible. Also the model provides detailed understanding of how the radial component of the magnetic field could greatly decrease our ability to obtain momentum reconstruction from the XTPC, and how to alleviate this by locating the XTPC as close as possible to the magnet pole piece.

In order to form the simple model, we define the magnetic field as follows: It is a cylinder, length 2L, of uniform field, B_z, directed along the RHIC beam axis, z. This is followed immediately by a disk of very small thickness, t, in which there is only radial magnetic field, Br, independent of z, whose magnitude increases linearly with radius, r. After the disk, a particle drifts through a field-free region of length D, measured along the z axis, whereupon it hits the first of the (eight) planes of the XTPC at z= L+D. This model will be solved exactly for the trajectories in the central TPC and the XTPC.

A. RELATION OF B_r TO B_z

To relate the strength of the two fields, consider the case where the disk is composed of high-permeability material like iron. Then imagine a hypothetical Gaussian surface which is a cylinder with axis along z and radius r. One planar face of the Gaussian cylinder is at z=0, the site of the primary vertex for the events produced by RHIC, and the other face is just beyond the "iron" disk. Since the divergence of the B field vanishes, so must the net perpendicular flux through the Gaussian surface vanish. Since B=0 at the large-z face, there is no contribution there. Also no flux penetrates the curved portions of the Gaussian cylinder, except inside the disk. The other flux penetration is at the face at z=0. Thus,

$$\pi r^2 B_z = 2\pi r t B_r \qquad (1)$$

or

$$t B_r = r B_z/2, \qquad (2)$$

so the line integral, at constant radius, of the radial component of B increases linearly with radius, and its value is given by the right-hand side of Eq.(2).

Later we will briefly compare the results using the model field with those we obtained from GEANT, using a field map for STAR supplied 10/94 (denoted ROSS3) by Ross Schleuter. The actual STAR geometry has an iron disk pole piece at either end of the solenoidal field, with a hole of ~90-cm radius in each pole piece. For the central interior of this solenoid the $B_z = 0.52$ Tesla. So the radial field integral at, e.g., 60 cm radius for the model field (no hole in "iron") would be

$$\mathrm{INT60} = 0.156 \text{ Tesla m}, \tag{3}$$

or

$$\mathrm{INT50} = (5/6) * 0.156 = 0.130.$$

We will retain this value for the integral while going to the limit that the disk thickness, t, is much less than L and D. Then in Section F we will modify this.

B. TRAJECTORY OF PARTICLE

We will describe the trajectory of a singly-charged particle of momentum p emitted at z=0 at the angle θ from the z axis. Recall that θ uniquely determines the pseudorapidity, but θ is more relevant to this primarily geometric problem. From z = 0 to L, the trajectory will be a helix, as considered in Ref. 1. The radius of the circular projection of this helix onto the x,y plane is

$$\rho = p \cdot \sin(\theta)/(0.3 \cdot B). \tag{4}$$

When it reaches the disk, starting at z=L, the trajectory will conform to the circular portion of Fig. 1, with radius of curvature, ρ_1. The radial component of p is the same on both sides of the disk. Quantities in Fig. 1 are related through

$$t/\rho_1 = 0.3 \cdot \mathrm{INT60} \cdot r/(0.6p_1), \tag{5}$$

analagous to Eq.(4). Before the disk, the two components of p_1 in the plane of Fig. 1 are p_z and p_ϕ. The angles are related by

$$\varepsilon = \alpha + \gamma = \alpha + \sin^{-1}(t/\rho_1 - \sin\alpha). \tag{6}$$

C. TWIST

In Ref. 1 the twist angle, τ, is defined and described. As a reminder, twist is the angle between the track and the radius extending from the z axis to the hit in the first plane, both projected onto the x,y plane. For no radial field, Section I, the twist is, to high accuracy, inversely proportional to the momentum, and is quite insensitive to θ.

As discussed in Ref. 1, the twist is the primary basis for determining the sign of the charge as well as the momentum of the particle. Changing the sign of the charge changes the sign of the twist. Twist also contributes to our ability to distinguish primary particles from secondaries. Thus, twist is vital to the physics that can be obtained from the XTPC tracks.

With the radial field of the present model, these same statements about the twist are still correct, except that for intermediate values of INT60 the twist depends somewhat more on θ when $p <\sim 0.5$ GeV/c. However, the twist is reduced by the radial component of B. That is, the twist is essentially related to the component, p_ϕ, after the disk in Fig. 1. If p_ϕ vanishes after the disk, then twist vanishes. The radial field always subtracts from this component, primarily due to the interaction of p_z with B_r. Furthermore, if INT60 could somehow be controlled independently of B_z we will see in Section F how the twist decreases linearly with increasing INT60, going through zero twist at a particular value of INT60.

D. CONDITIONS FOR ZERO TWIST

What is the value of INT60 for which twist vanishes? From Fig. 1, if γ=0, then all hits in the XTPC will be along the same radius vector perpendicular to the z axis, and twist will vanish. Eq.(6) shows that this will occur when

$$t/\rho_1 = \sin\alpha \tag{7}$$

Using, as in Ref. 1, β as the angular segment of the circle of radius ρ traversed by the particle from z=0 to z=L (before the disk), one can see that the components of ρ_1 before the disk in Fig. 1 are

$$p_\phi = p \cdot \sin(\theta) \cdot \sin(\beta/2) \tag{8}$$

and

$$p_z = p \cdot \cos\theta \tag{9}$$

while

$$p_r = p \cdot \sin(\theta) \cdot \cos(\beta/2). \tag{10}$$

A similar kind of diagram drawn for the x,y projection of the part of the trajectory between z = 0 and L shows that

$$\text{pole\_radius} = 2\rho\sin(\beta/2), \tag{11}$$

where pole_radius means the perpendicular distance from the z axis to the place where the particle first hits the disk. Combining Eqs. (5), (7), (8) and (11) gives Eq. (2). Thus, for the critical value of INT60, given by Eq. (3), the twist vanishes. That is, projected onto the x,y plane, the track is along a radius vector.

Here we have an important, but unwelcome, result. For the model field (thin "iron" wall, no hole), the twist is identically zero, regardless of p, θ, L, D or strength of B_z.

E. ANGLE BETWEEN MOMENTUM AND z AXIS, BEYOND DISK.

In the case that $B_r = 0$, as in Ref. 1, the angle between the momentum and the z axis is everywhere the same, θ. For nonzero B_r, denote the angle between the momentum after the disk and the z axis as θ' (in three dimensions, not in projection). One can show that

$$\tan\theta' = (p_1\cos\gamma)^{-1}\sqrt{(p_r^2 + p_1^2\sin^2\gamma)} \tag{12}$$

Then if the free-drift distance, D, were zero, the twist, τ_o, for a particle would be

$$\tan\tau_o = (p_1\sin\gamma)/p_r, \tag{13}$$

which will be used later.

F. TWIST FOR INT60 LESS THAN CRITICAL

In the actual STAR geometry there is the hole in the iron sheet which permits the radial field to be spread over a significant region of z, near z=L. This affords a means of obtaining significant twist in the real case - viz., by moving the XTPC close to the iron pole tip so part of the line integral of the radial field is not traversed before reaching the XTPC. In this way, INT60 can be made less than critical.

Thus, we evaluate the twist for the case that INT60 has a value less than for Eq.(3). This twist is obtained geometrically from a triangle (not illustrated) whose three sides are pole_radius, $D \cdot \tan\theta'$, and hit_radius (the x,y projection of the distance from the z axis to the hit in the first plane of the XTPC). This hit_radius is calculated from the components of p_1 beyond the disk (obtained from γ in Fig. 1 and the fact that the component pr beyond the disk is the same as Eq.(10)). Thus the x and y coordinates of the hit are

$$\text{x\_hit} = D \cdot \tan\theta' \cdot \sin\tau_o \tag{13a}$$

$$\text{y\_hit} = \text{pole\_radius} + D \cdot \tan\theta' \cdot \cos\tau_o \tag{13b}$$

From these, the twist is obtained from said triangle as

$$\text{twist} = \tan^{-1}(\text{x\_hit}/\text{y\_hit}) - \tau_o \tag{14}$$

Plots of twist vs momentum are shown in Figs. 2(a) and 2(c). These are shown for theta = 2, 8 and 14 degrees, which nearly cover the range subtended by the XTPC, for high-p particles. Figure 2 is for L+D = 3.85 m. It also has INT50 = 0.1017, which matches rather well (cf. Section J) the results we obtained from ROSS3 and GEANT (but see Section J for improvement). The line in Fig. 2(a) is 2.813/p. It describes the twist to within 2.5% for p> = 1 GeV/c and theta = 8 degrees, Fig. 2(c). This line passes exactly through the point at p= 10, θ= 8. Figure 2(b) shows how $\tau \cdot p$ depends on θ, with curves representing p = 0.20, 0.25, 0.30, 0.35, 0.40, 0.50, 0.70, 1, 2, 5 and 10 GeV/c. These momenta were used for all the calculations discussed here. The curves in Fig. 2(b) go monotonically with p.

As p is made smaller than 0.2, the twist continues to increase. For all three cases in this work, as momentum decreases, the twist becomes larger than 90°. Then the track appears to be going backwards, with the radius of the hit in the first plane being larger than the radius for the last plane. This is also observed occasionally in our GEANT AuAu simulations with the realistic field map.

Figure 3 shows the dependence of the product $\tau \cdot p$ (p>>1) on the strength, INT50, of the radial field integral at 50 cm radius. Thus, for a given θ, the twist is linear with INT50 to high accuracy, and vanishes at INT50= 0.13 Tesla m, the same value as from Eq.(3) and Section D. Figure 3 shows θ = 2, 8 and 14 degrees, and each of these is linear, converging on zero at the same INT50. At INT50= 0, the value for θ = 2 is 0.99 times that for θ = 8, while the value for θ = 14 is 1.02 times that for θ = 8.

G. HIT RADIUS (FIRST PLANE)

Here we discuss the x,y projection of the radius of the hit in the first plane of the XTPC. For large-momentum particles the trajectory from vertex to XTPC is nearly a straight line, in which case we would expect the projected radius of the hit in the first plane of the XTPC to be at $(L+D) \cdot \tan\theta$. Thus, we expect a plot of radius/($(L+D) \cdot \tan\theta$) to be unity for large p and to decrease as p is reduced. This is seen in Fig. 2(d). Again, the points at θ = 2, 8 and 14 are close together, coalescing for p>~1 GeV/c. Figure 2(d) will be the primary basis for experimentally evaluating θ (thus, pseudorapidity) as discussed below.

H. TRACK LENGTH/ HIT RADIUS

Again, both lengths are the x,y projections. The ratio of track length to hit radius can serve to distinguish tracks of primary particles from those of secondaries. The track length is determined by θ', Eq.(12). The ratio θ'/θ is shown in Fig. 2(f). Incidentally, the tracklength would be zero if $\theta' = 0$.

The track length has a different dependence on where the particle is born than does the hit radius. For $B_r = 0$, e.g., the track length is independent of where the particle is born. In general, the ratio, tracklength/radius distinguishes primaries from secondaries. For a primary of larger momentum this ratio becomes $\delta/(L+D)$, where δ is the thickness, along z, of the XTPC. The ratio decreases for smaller momenta, as seen in Fig. 2(e).

I. RESULTS FOR NO RADIAL MAGNETIC FIELD

If INT60 could be made vanishingly small we would have the other limiting condition, to be contrasted with INT60 being critical. This case of INT60 = 0 is the subject of Ref. 1. This condition could be nearly achieved realistically by placing the XTPC inside the STAR solenoid, before the magnetic pole tip.

By setting INT60 = 0 in the above expressions, the results of Ref. 1 are reproduced. These are summarized in Fig. 4 which has the same layout as Fig. 2. Again, (L+D) = 3.85 m. In

Fig. 4(a), the twist is only slightly dependent on θ. This is seen in Fig. 4(b) where, for all momenta, $\tau \cdot p$ has the same slight variation as for the high-momentum limit of Fig. 2(b). The line in Fig. 4(a) is 12.921/p, passing exactly through the point at p = 10, θ = 8.

The primary difference from Fig. 2(a) is the magnitude of the twist, which is about a factor of 4.6 larger for INT60 = 0. This is because of the untwisting effect of the disk of radial B.

The ratio of hit radius to (L+D)tanθ is almost the same in Figs. 4(d) and 2(d). Thus the experimental determination of θ, or pseudorapidity, has nearly the same effectiveness for both.

The ratio of track length to hit radius has the opposite departure from their identical high-momentum limits in Figs. 4(e) and 2(e).

Figure 4(f) shows that the values of θ are the same everywhere, in contrast with Fig. 2(f).

J. EFFECT OF NONLINEARITY OF RADIAL-FIELD INTEGRAL

In this model with no hole in the "iron" disk, the radial-field integral is exactly linear with radius, Eq.(2). In the realistic field map, ROSS3, this integral is nearly linear, as found by numerical integration from z = 0 to z_f at constant radius. The value of z_f represents the location, L+D, of the first plane of the XTPC.

Figure 5 shows this nonlinearity of ROSS3. The ordinate is (integral at radius r)/(integral at r = 0.45 m) $*$ (0.45 m)/r. The abscissa is this radius, r. Concerning the abscissa, one can consider the angle, arctan(r/3.32), with 3.32 m being the value of z where the radial component of field is most intense[2]. Thus, the abscissa is almost linear with the value of θ of high-momentum particles. The curves would all be unity if the integral were exactly linear with r. The nonlinearities are a few percent for $z_f > 3.8$ m, and they decrease with z_f.

This nonlinearity can be incorporated into the model by using the appropriate curve in Fig. 5 to choose a (slightly different) value for integral/r_d according to the radius, r_d, at which the particle reaches the disk of radial field - i.e., the pole_radius of Eq.(11).

The results of this nonlinearity are seen in Fig. 6. The primary effect is to invert the θ dependence of the twist in Fig. 6(b), compared to Fig. 2(b). Thus the twist for given p is monotonically decreasing with θ in Figs. 6(a) and 6(b), and monotonically increasing in Figs. 2(a) and 2(b). This makes the results in all parts of Fig. 6 very similar, both qualitatively and quantitatively, to the results we obtain with ROSS3 and GEANT.

The line in Fig. 6(a) is 2.783/p, passing exactly through the point at p=10, θ = 8.

K. COMPARISON OF MODEL RESULTS WITH GEANT RESULTS

The behavior of all aspects of Fig. 6 compare well, both qualitatively and quantitatively, with analogous plots of our results using the realistic magnetic field, ROSS3, and GEANT. We made partial GEANT plots like portions of Figs. 6(a), 6(d) and 6(e). Detailed comparison will not be discussed here, except to say that the agreement was good. The same selection of eleven momenta and seven angles θ was used as our input to GEANT. The GEANT runs were made with all physics turned off. It was necessary to run with AUTO=0, without further inputs of associated parameters, in order to obtain accurate results, in spite of the warnings in the GEANT manual to use AUTO=1. Also, in order to obtain GEANT results such as the twist, our analysis program was needed, and this had not yet been upgraded to analyze properly tracks with larger twist, such as occurs for p<~ 0.5 GeV/c and L+D= 3.85 m. It was also necessary to select azimuthal angles of launched protons such as to be certain that tracks from different values of p and θ were far enough apart as to avoid interference among tracks. There was not readily available a worthwile way to make GEANT plots analogous to Figs. 6(b), (c) and (f). However, their properties could be inferred from a careful examination of our GEANT analogues of portions of Figs. 6(a), 6(d) and 6(e).

L. EMPIRICAL VALUES OF INT60

At three values of L+D (3.85, 4.00 and 6.15 m), our values of twist from GEANT, using ROSS3, were compared to those from this model. One would expect a difference since the realistic B_r is not just restricted to values of z near the pole tip, and B_z is not a step function at the pole tip. The best match was found with INT60 about 4% less than the values obtained from direct numerical integration of ROSS3. The value, 6.15 m, is the L+D for the earlier planning for XTPC.

With INT60 taken as ≈4% less than that of ROSS3, this being the only adjustable parameter in the model, there is good agreement of the model results with those we obtained with a realistic field map, ROSS3, plus GEANT. The nonlinearity effect in Fig. 5 was obtained numerically from ROSS3, with no adjustment.

It is believed that this model, a sample of whose results are given in Fig. 6, can now be used to represent the important aspects of the trajectories in the real system of STAR central TPC plus XTPC. It is simple enough to give understandable answers for a wide variety of circumstances. It is useful for understanding how to formulate a tracker algorithm. It is useful for anticipating effects of changes in parameters. Of course, we are using GEANT calculations for the final analysis.

M. DEPENDENCE OF TWIST ON L+D

Figure 3 demonstrates the need to place the XTPC as close to the solenoid's pole piece as possible. In the limit of large L+D, the value of INT50 for the ROSS3 field map approaches the critical value of 0.130 where the twist vanishes. By moving the XTPC closer to the solenoid, less of this full integral is experienced by particles before reaching the XTPC, so the twist is increased, as indicated by Fig. 3. In order to quantify this, Twists were evaluated from this disk model for various L+D. The results are given in Fig. 7. The effects of the nonlinearity of the radial-field integral were included by using Fig. 5 for each value of z_f (i.e., L+D). The value of L+D=3.85 m, used in the other Figures, is such that the main body of the XTPC is just not touching the iron of the pole piece[3] of the central TPC. This is chosen to make the twist as large as possible.

Of course, if there were not multiple scattering by the materials enroute between the primary vertex and the XTPC, there would be very little uncertainty in the measured twist, so smaller twist could be tolerated. However, our runs with GEANT show that this multiple scattering is a major problem. It is mainly caused by the beam pipe, now that the Vertex Position

Detector (a former major source of multiple scattering) is planned to be beyond the XTPC. There are also important contributions of multiple scattering from the end cap of the Silicon Vertex Detector. For these reasons, examination of Fig. 7 shows that L+D must be made as small as possible.

To emphasize again, because of multiple scattering, the extent of the physics obtainable from XTPC increases rapidly as the twist increases for a given momentum. Figure 7 shows that the twist increases rapidly as the XTPC is placed closer to the magnet pole piece. Hence, the XTPC must be as close as possible to the central TPC.

N. RECONSTRUCTION OF PSEUDORAPIDITY AND MOMENTUM FROM EXPERIMENT

In the experimental situation, the complete description of the geometrical properties of any track is the specification of the radius of the hit in the first plane, the twist of the track and the length of the track. (Each of these is in the x,y projection). No other information is significant. For example, the azimuth of the hit in the first plane has no significance since there is no way to know independently the azimuth of origin of the particle.

How can we use this information to obtain the momentum and its direction, θ, of particles from the primary vertex? Examination of Fig. 6(a) shows that the twist is nearly a unique indicator of the momentum. However, there is nonnegligible dependence on θ, Figs. 6(b) and 6(c). On the other hand, Fig. 6(d) shows that the radius of the hit in the first plane of XTPC is nearly a unique measure of $\tan\theta$, once one knows the momentum, p. The word "nearly" is appropriate because there is up to a few percent dependence of the height of those curves on θ.

The following procedure works very well to determine p and θ accurately, using only twist and radius. First, we make a table associated with the, e.g., seven values of θ and eleven values of momentum used to make these plots. The table contains twist (as in Fig. 6(a)) and (radius/[(L+D) $\cdot$ $\tan\theta$]) (as in Fig. 6(d)) at each of these 77 points. For short, designate this latter quantity as RADBY, the ordinate in Fig. 6(d). In order to interpolate along constant θ in Fig. 6(a), we note that the plot is nearly linear, so we interpolate linearly on log(twist) vs log(p). This means that

$$\tau/\tau_1 = (p/p_1)^{-k} \qquad (15)$$

where the subscript 1 means values in the table at the nearest momentum below the momentum, p, for which τ is to be evaluated. The exponent, $k>0$, at that p and τ, is obtained by linear interpolation between the two values of k obtained from table values of θ on either side of the θ being considered. Thus for the given twist and a tentative value of θ, a tentative value of p can be found from the table and Eq.(15). Designate this process as X.

In order to obtain a better theta for this tentative p, we interpolate linearly between table values of RADBY vs θ and p, Fig. 6(d). Designate this process as Y.

The reconstruction proceeds as follows. Start with the experimental value of twist and experimental value of radius of first-plane hit. Use the twist in process X and an initial value of $\theta = 8$ (arbitrary) to get an initial value of p. Use that p and a first RADBY (e.g., estimated from

Fig. 6(d)) in Y to get a second approximation to θ. Use that second θ and experimental twist in X to get a second p. Continue iterating this process until convergence, which occurs after only a couple of iterations. In fact, the convergence was so good, that quite arbitrary starting values of p and RADBY could be used, while still obtaining rapid convergence.

A simple program of this kind has been made, and here are some examples of the reconstruction process. As the first example, consider values in the high-momentum region where Fig. 6(a) is nicely linear, and where Fig. 6(d) is quite insensitive to p or θ. For the values of p= 7.5 and θ = 13 it was determined by using this same kind of interpolation[4] that the resulting twist= 0.31078 degrees and radius= 88.849 cm. This twist and radius were the input parameters[5] to the program. The rather wild (compared to Fig. 6) starting values of p=20 and RADBY=0.5 were used as a drastic test of convergence. The successive values of p, RADBY, θ; p, RADBY, θ; etc. were found to be the following: 20, 0.5, 24.8; 3.376, 0.9993, 13.004; 7.499, 0.999599884, 13.000001; 7.4999995, 0.99959999996, 13.0000000005; 7.4999999999, 0.99600000000, 13.0000000000, etc. Thus the expected solution of p= 7.5 and θ = 13 was obtained accurately and quickly.

A variety of pairs of p and θ in this high-momentum region was used with similar results. Other regions were investigated as well, but we will give only one more example.

Take the case of p= 0.275, θ = 3, in the rapidly sloping regions of Figs. 6(a) and 6(d). Here the "experimental" values for starting the process are twist= 16.4017... and radius = 16.4917... Again the starting values were rather wild, considering Figs. 6(a) and 6(d), viz., p = 0.25 and RADBY= 1. Again, the successive values of p, RADBY, θ; are 0.25, 1, 2.45; 0.2753, 0.8179, 2.998; 0.275001, 0.817352, 2.999991; 0.275000005, 0.817350009, 2.99999997; 0.27500000002, 0.81735000004, 2.9999999999; ... Again, the convergence is accurate and rapid, even in this more demanding region.

The method of analysis of p and θ that we presently use with GEANT does not iterate, so it makes approximations that are most accurate at momenta above 1 GeV/c where the curves in Fig. 6 are simplest. It will not slow the analysis significantly to incorporate the present few iterations in order to extend the momentum range and obtain better accuracy.

In the case of no radial field, the reconstruction is much simpler. Ref. 1 describes how it can be done in one step from the twist. The essential reason is that Fig. 4(b) is essentially a single curve for all momenta, whereas Fig. 6(b) is not.

O. REJECTION OF SECONDARY PARTICLES

To this point, the length of the track has not been included in the analysis. As mentioned in Section H, the ratio of track length to hit radius can serve to distinguish a track originating at the primary vertex from one originating elsewhere. This involves the results in Fig. 6(e).

An initial, simple screening can be made to reject a large fraction of the secondaries before the analysis of Section N is even commenced. This is illustrated in Fig. 8(c), made with the same conditions as Fig. 6, the GEANT look-alike. Figure 8 contains all the relevant geometrical measurables of a track, viz., twist, length and radius. Each curve is for a single θ.

The two outside curves of Fig. 8(c) are for nearly the limiting values of θ which will reach the XTPC, so these outside curves are nearly the boundaries of the region that primaries can occupy. Thus, an initial screening can exclude all tracks outside this "primary" region, since they must be secondaries.

However, we must be careful for small momenta. The pole_radius, Eq.(11), is always < $L \cdot \tan\theta$, with equality in the limit of small β (i.e., large p). Thus, for small p, larger values of θ can get through the hole in the pole tip and reach the XTPC. Hence, for small p (large twist) the limiting θ is larger than the ~14° of larger p, and the "primary" region of Fig. 8(c) extends farther downwards (larger θ) at larger twist.

Figure 8(a) has the same conditions as Fig. 2 (exactly linear radial integral), and Fig. 8(b) has the same conditions as Fig. 4 (no radial field). Note how thoroughly secondaries could be rejected (how narrow the "primary" region) by this initial screening if the radial integral were exactly linear with radius, so Fig. 8(a) applied. If there were a vanishing radial integral, Fig. 8(b), the "primary" region would be vanishingly small

Consider Fig. 8(c) in more detail. The three points at the lower right are for the smallest p, 0.2. The next triplet of points is for p = 0.25, the next for 0.3, etc. On any one curve (fixed θ), momentum decreases monotonically, going from left to right. Along a fixed-θ curve the radius is $f \cdot \text{const} \cdot \tan\theta$, where f is the ordinate in Fig. 6(d), and varies from about 0.67 (depends weakly on θ) at p= 0.2 to $f \to 1$ at p>~ 1. Thus, once θ and p are known, Section N, the required radius for this track to be a primary is known.

By this means of checking the radius, once θ and p are known, we have the capability to eliminate all wrong-radius secondaries that survived the preliminary screening.

Figure 8(c) provides another way to describe how p and θ of primaries are determined. A given primary track is a single point in Fig. 8(c) in the "primary" region. The angle θ is determined by noting which of the fixed-θ curves it lies on. The distance along that curve determines p. Every point in the "primary" region corresponds to a possible primary. This method of explanation using Fig. 8 shows the logic, but Section N is a better numerical way to find p and θ. From Fig. 8(b) alone, one might conjecture, quite erroneously, that it is not possible to evaluate θ accurately for the case of negligible radial field.

P. POSSIBLE BACKSWIMMING

In Ref. 5, it was suggested that secondaries can be rejected on the basis of backswimming the three-dimensional track, starting with its hit radius and initial three-dimensional orientation, through the magnetic field to find at what radius it crosses the plane, z=0. If this radius were acceptably small, the track would be considered to be a primary. To backswim requires knowing the momentum in the field. The method of analysis suggested in Ref. 5 is more involved than that described here. For example, for some tracks repeated backswimming is used to evaluate momentum.

However, after determining p, Section N, a single backswimming could, in principle, be used as an alternative for Section O for secondary rejection. The location and orientation of the initial backswimming momentum vector would be given by reversing the direction and charge of the three-dimensional track. The momentum for the backswim would be that just mentioned. If the radius at the plane z=0 were sufficiently small, the track would be accepted as a primary.

By comparison, the method proposed in Section O for secondary rejection is done quickly in one step. Backswimming has several problems. It takes considerably longer since several thousand small steps must be taken for each track. It involves the problem of deciding what step size to use: If the step size is too large, the result is too coarse; if the step size is too small, the result is subject to roundoff error, and it takes longer. There is also the need to reproduce the effect of the energy loss, dE/dx, experienced in the forward swim, especially for low-energy particles. For the present method of analysis, the effect of energy loss is effectively contained in the table. That is, the energy loss can be turned on, with other physics turned off, when the selected values of p and θ are run through GEANT to determine the table. The energy loss is rather small for most of the cases considered here, and will have a small effect on the table.

The only possible reason for using backswimming rather than Section O to identify secondaries is that the former might somehow be less upset by multiple scattering along the trajectory before the track in question. This seems unlikely. Both approaches start with the same information, the track geometry.

Q. LIMITS TO REJECTION OF SECONDARIES

Even disregarding multiple scattering, there are some limits to the extent to which secondaries can be rejected. The reason is that even if one knows exactly the twist, length and radius of the track, the momentum can not be determined without additional information unless the particle is assumed to have originated from the known primary vertex.

One type of secondary that cannot be identified is one born somewhere along a possible trajectory of an imaginary primary, and born with all the same properties that this imaginary primary track had at this point of birth of the secondary. No method using only track geometry in the XTPC will identify such a secondary.

A less trivial type of secondary can be discussed by considering backswimming. Imagine a given primary track in the XTPC with momentum, p_1. Imagine backswimming from this track using some other (incorrect) momentum magnitude, p_2. Then a secondary born with the reverse of the vector momentum (magnitude p_2) that this backswum track has anywhere along its path would be indistinguishable from the imaginary primary with the original momentum, p_1.

Nevertheless, the probability of unidentifiable secondaries is rather small in the real situation. For a full energy HIJING AuAu event, GEANT shows roughly only half again as many secondaries into the XTPC as primaries into the XTPC. Only a small fraction of these secondaries can be in the category just described as unidentifiable. Thus the ratio of primaries to leaking secondaries is large.

Preliminary tests, with GEANT, of secondary rejection using the pre- analysis rejection of Section O were very encouraging. However, this older tracker did not find tracks with larger twist, where the problem is more demanding. On the other hand, the radius check, Section O, has not yet been implemented.

R. EFFECTS OF MULTIPLE SCATTERING ON RECONSTRUCTION RESOLUTION AND SECONDARY REJECTION

It was mentioned in Section M that multiple scattering from the beam pipe and the other materials inside the central TPC are the major limitation on the performance of the XTPC. Multiple scattering smears somewhat the twist, the tracklength and the radius on which the analysis depends. While this can be approximated without GEANT, the only certain method of evaluation is with GEANT, using the realistic map of materials. We are doing this now.

It is interesting to note that if all multiple scattering took place very near the primary vertex, the reconstruction in Section N would still give correctly the momentum after the scattering. The reconstructed θ would be the corresponding polar angle (nearly θ) after the multiple scattering.

REFERENCES

1. J. Draper, D. Cebra, J. Romero, STAR NOTE 172, May, 1994.

2. This same 3.32 m is used for L in the present calculations.

3. The effects of the fringe magnetic field on the drift of the electron cloud in the XTPC have been estimated. They appear to be significant, but tolerable.

4. The correct values could have been calculated directly, rather than using this interpolation. However, we wanted to use this same interpolation in order to expect nearly perfect numerical agreement if the convergence is rapid and accurate. A more sophisticated method of interpolation would have ameliorated this.

5. The full accuracy of the computer, 12 digits, was used naturally to obtain the input. There is no reason to show most of these digits, except at those places in the iterations that reveal how strong is the convergence.

6. I. Stancu, STAR Workshop, April, 1992, unpublished.

FIGURE CAPTIONS

Fig. 1. Projection of trajectory onto the plane perpendicular to the radius vector; the plane contains the point where the trajectory first reaches the disk, and contains an imaginary line through this point and parallel to the z axis. The disk of thickness, t, contains the radial field. Radius vector here means the x,y projection.

Fig. 2. Results for L+D= 3.85 m, optimal INT60 (Section L), and strictly linear dependence of radial-field-integral vs r. The following symbols have the same meaning in all Figures in this work: + for $\theta = 2$, o for 8, and x for 14 degrees. They are in all panels here except 2(b). (a) Twist vs momentum. (b) Ordinate is twist $\cdot$ momentum divided by its value at $\theta = 2$. Each curve is for constant p. The curve heights change monotonically with p. (c) The curve connects points with $\theta = 8$. (d) Radius/[(L+D) $\cdot$ tanθ] vs p. (e) Tracklength/radius $\cdot$ (L+D)/δ vs p. The XTPC thickness (along z) is δ= 0.70 m. (f) θ'/θ vs p.

Fig. 3. Twist $\cdot$ p vs INT50, the radial field integral at 50 cm radius, for $\theta = 2$, 8 and 14.

Fig. 4. Same as Fig. 2, except zero radial magnetic field.

Fig. 5. Nonlinearity of radial-field integral in ROSS3 field map. This integral is from z = 0 to $z = z_f$ at constant radius, r, the abscissa. Curves are labeled with z_f in cm. (a) $z_f >= 3.8$ m. (b) $z_f <= 3.8$ m.

Fig. 6. Same as Fig. 2, but includes effect of small nonlinearity in ROSS3 radial-field integral, Fig. 5. Now the direction of some dependences on θ is reversed, as discussed in Section J. Curves in this Figure are quite like GEANT-produced curves using the ROSS3 field map.

Fig. 7. Twist $\cdot$ p at large p vs (L+D) for $\theta = 8$ degrees. The effects of nonlinearities in Fig. 5 are included. Shows the importance of placing the XTPC as close as possible to the central TPC's magnet pole piece.

Fig. 8. Tracklength/hit_radius $\cdot$ (L+D)/δ vs twist. Each curve is for a fixed $\theta = 2$, 8 or 14 degrees. The eleven momenta are labeled as usual. A track from a primary particle emitted at a given θ, must lie on the curve for that θ. (a) Same conditions as for Fig. 2. (b) Same conditions as for Fig. 4. (c) Same conditions as for Fig. 6.

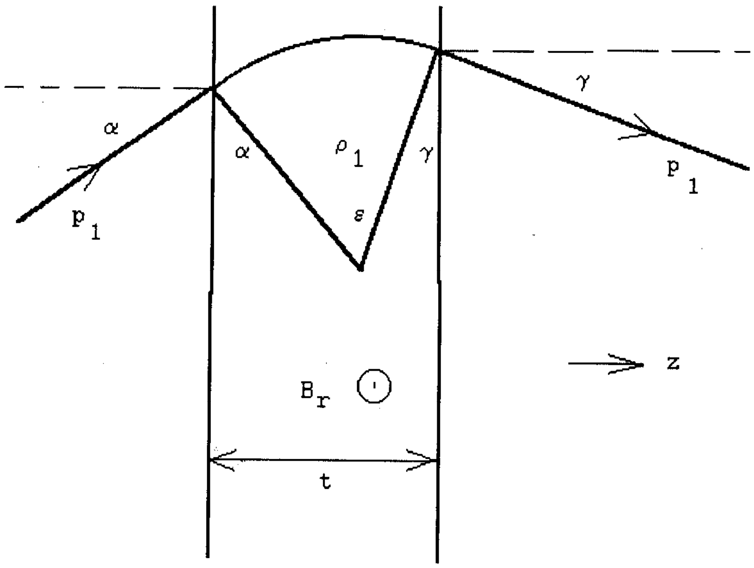

1

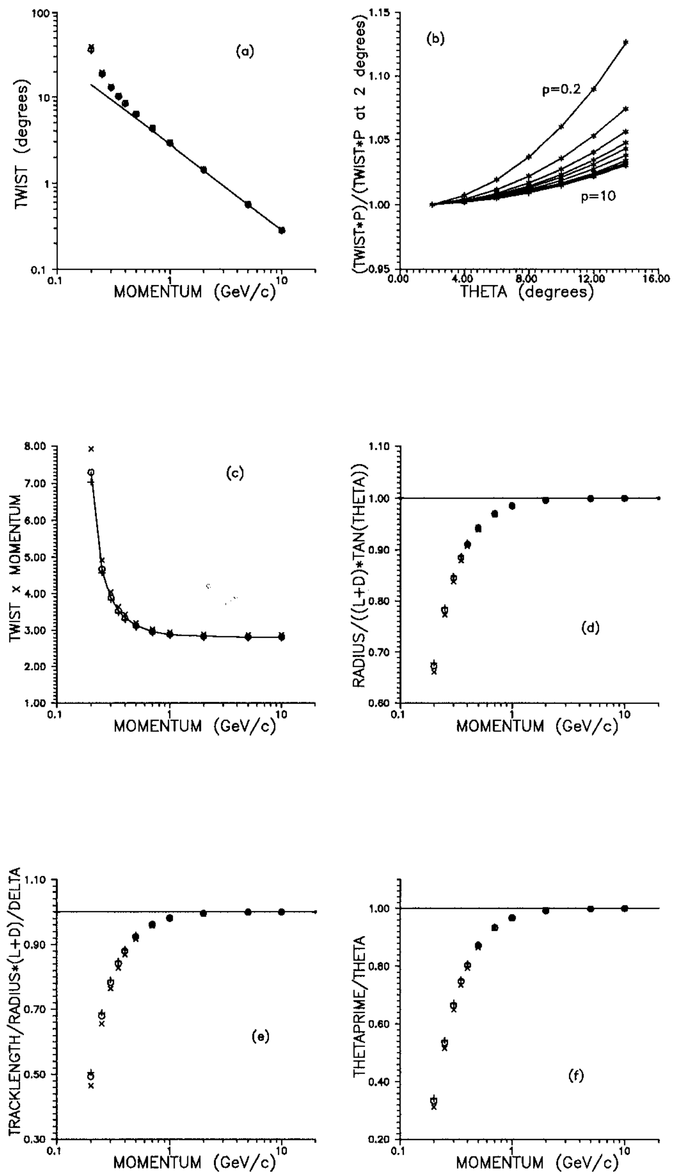
(a)
TWIST (degrees)
MOMENTUM (GeV/c)
(b)
(TWIST*P)/(TWIST*P at 2 degrees)
p=0.2
p=10
THETA (degrees)
(c)
TWIST x MOMENTUM
MOMENTUM (GeV/c)
(d)
RADIUS/((L+D)*TAN(THETA))
MOMENTUM (GeV/c)
(e)
TRACKLENGTH/RADIUS*(L+D)/DELTA
MOMENTUM (GeV/c)
(f)
THETAPRIME/THETA
MOMENTUM (GeV/c)

2

3

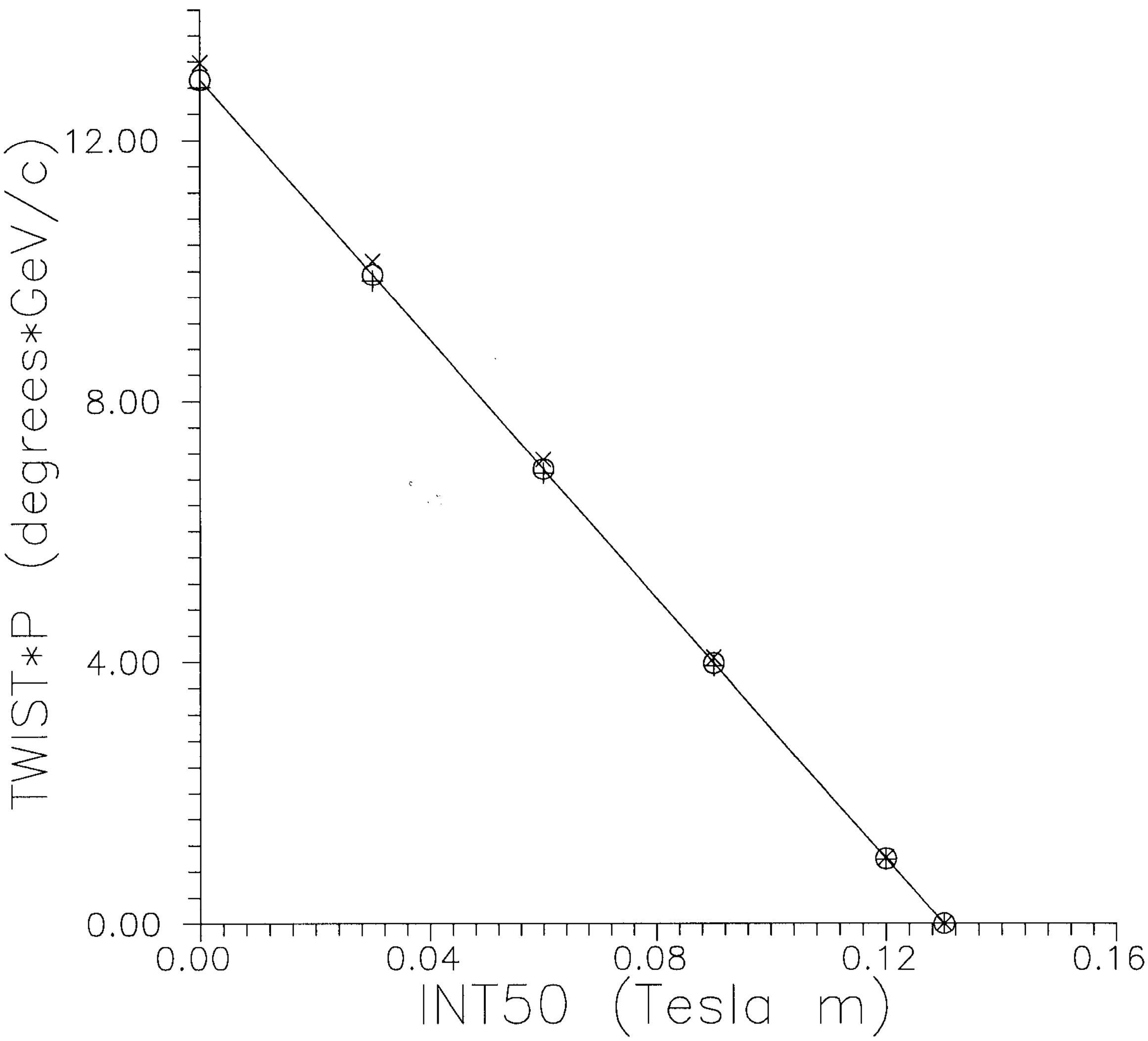
TWIST*P (degrees*GeV/c)
12.00
8.00
4.00
0.00
0.00
0.04
0.08
0.12
0.16
INT50 (Tesla m)

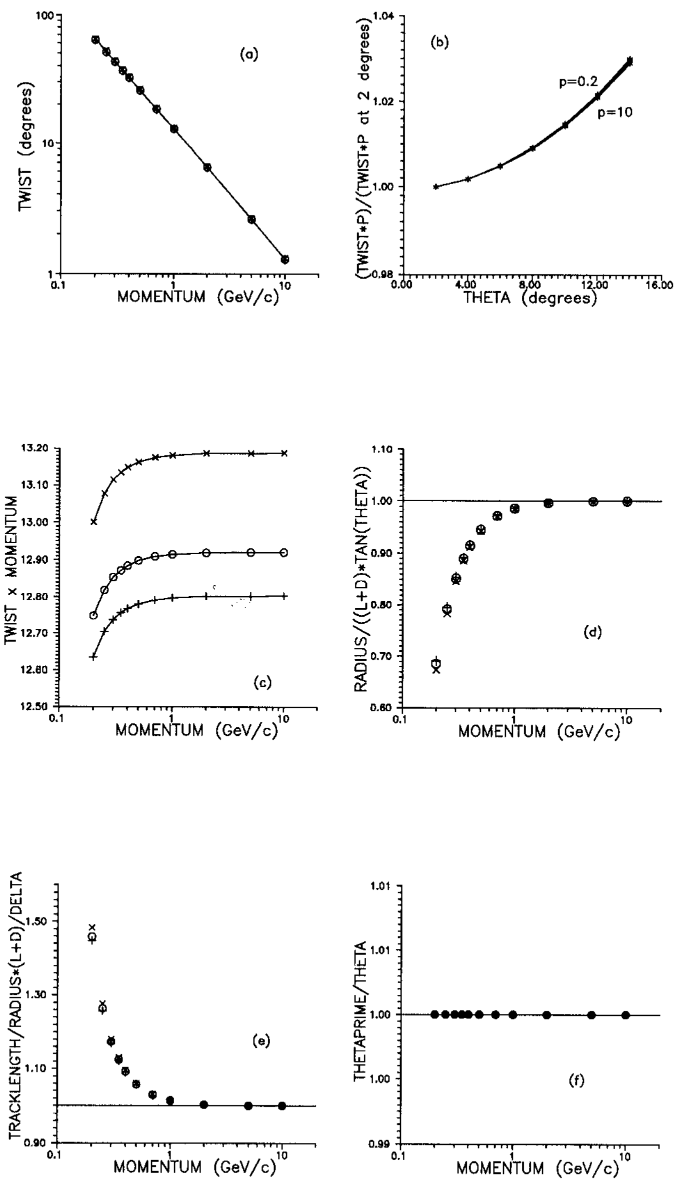
(a)
TWIST (degrees)
MOMENTUM (GeV/c)
(b)
(TWIST*P)/(TWIST*P at 2 degrees)
THETA (degrees)
p=0.2
p=10
(c)
TWIST x MOMENTUM
MOMENTUM (GeV/c)
(d)
RADIUS/((L+D)*TAN(THETA))
MOMENTUM (GeV/c)
(e)
TRACKLENGTH/RADIUS*(L+D)/DELTA
MOMENTUM (GeV/c)
(f)
THETAPRIME/THETA
MOMENTUM (GeV/c)

4

5

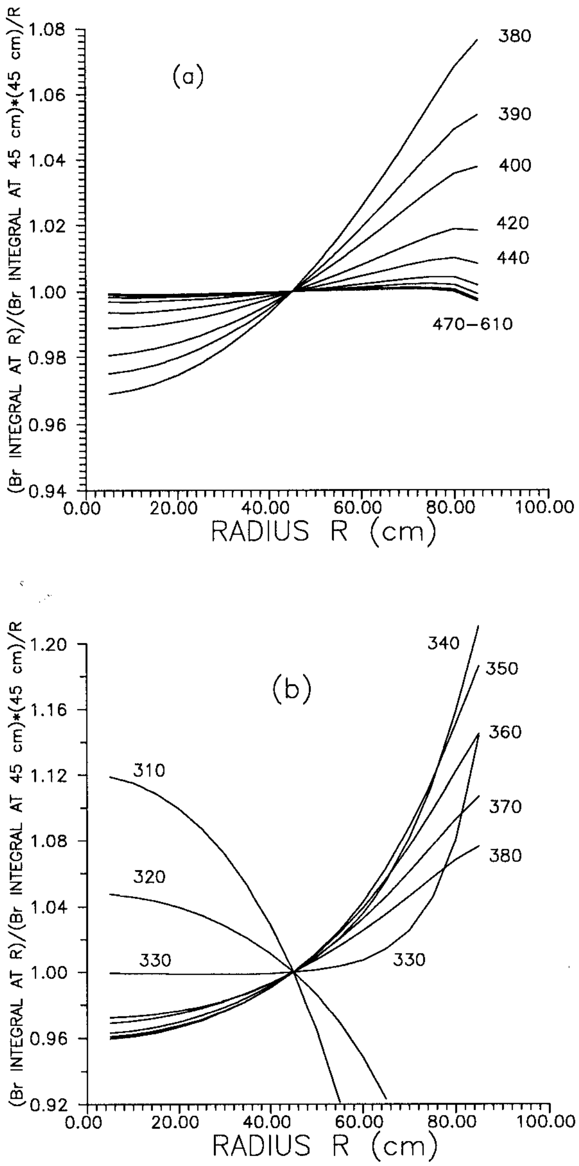
(a)
(Br INTEGRAL AT R)/(Br INTEGRAL AT 45 cm)*(45 cm)/R
RADIUS R (cm)
380
390
400
420
440
470–610
(b)
(Br INTEGRAL AT R)/(Br INTEGRAL AT 45 cm)*(45 cm)/R
RADIUS R (cm)
340
350
360
370
380
310
320
330
330

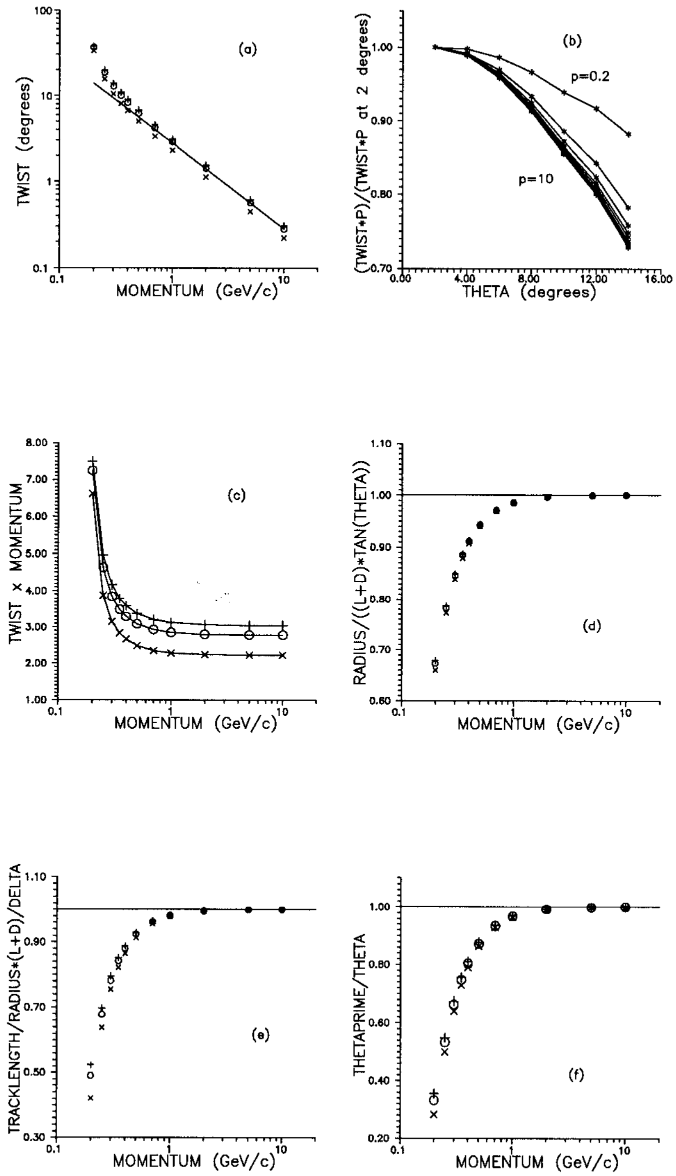
(a)
TWIST (degrees)
MOMENTUM (GeV/c)
(b)
p=0.2
p=10
(TWIST*P)/(TWIST*P at 2 degrees)
THETA (degrees)
(c)
TWIST x MOMENTUM
MOMENTUM (GeV/c)
(d)
RADIUS/((L+D)*TAN(THETA))
MOMENTUM (GeV/c)
(e)
TRACKLENGTH/RADIUS*(L+D)/DELTA
MOMENTUM (GeV/c)
(f)
THETAPRIME/THETA
MOMENTUM (GeV/c)

6

7

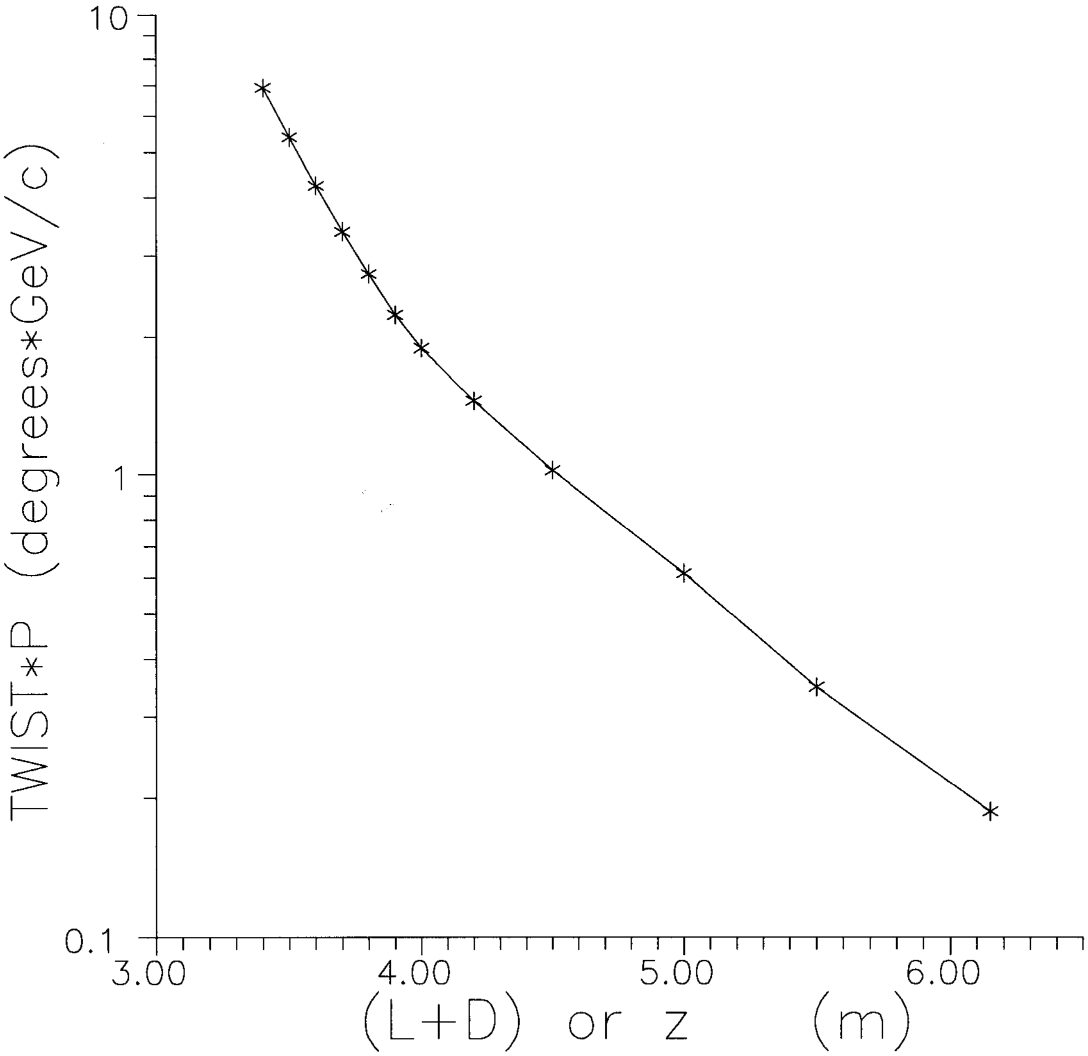

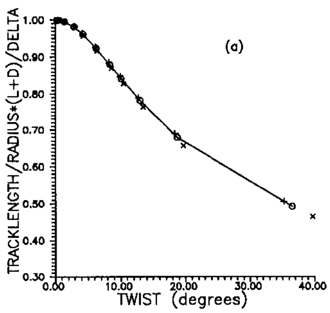
(a)
TRACKLENGTH/RADIUS*(L+D)/DELTA
1.00
0.90
0.80
0.70
0.60
0.50
0.40
0.30
0.00
10.00
20.00
30.00
40.00
TWIST (degrees)

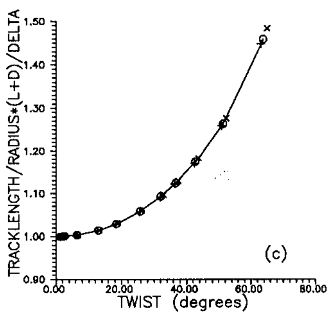
(c)
TRACKLENGTH/RADIUS*(L+D)/DELTA
1.50
1.40
1.30
1.20
1.10
1.00
0.90
0.00
20.00
40.00
60.00
80.00
TWIST (degrees)

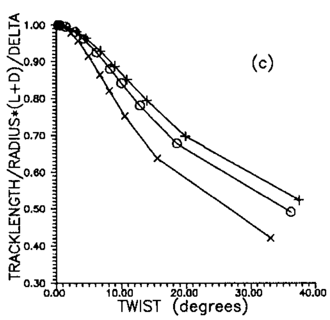
(c)
TRACKLENGTH/RADIUS*(L+D)/DELTA
1.00
0.90
0.80
0.70
0.60
0.50
0.40
0.30
0.00
10.00
20.00
30.00
40.00
TWIST (degrees)

8